

PAPER • OPEN ACCESS

Cooperative engulfment of nanoparticles by membranes and vesicles

To cite this article: Arash Bahrami and Amir H Bahrami 2024 *New J. Phys.* **26** 103012

View the [article online](#) for updates and enhancements.

You may also like

- [Engulfment of ellipsoidal nanoparticles by membranes: full description of orientational changes](#)
Jaime Agudo-Canalejo
- [The Impact of Tidal Migration of Hot Jupiters on the Rotation of Sun-like Main-sequence Stars](#)
Shuai-Shuai Guo
- [Metal Pollution in Sun-like Stars from Destruction of Ultra-short-period Planets](#)
Christopher E. O'Connor and Dong Lai



PAPER



Cooperative engulfment of nanoparticles by membranes and vesicles

OPEN ACCESS

RECEIVED
11 June 2024REVISED
16 September 2024ACCEPTED FOR PUBLICATION
27 September 2024PUBLISHED
10 October 2024

Original Content from
this work may be used
under the terms of the
[Creative Commons
Attribution 4.0 licence](#).

Any further distribution
of this work must
maintain attribution to
the author(s) and the title
of the work, journal
citation and DOI.

Arash Bahrami¹  and Amir H Bahrami^{2,3,*} ¹ School of Mechanical Engineering, College of Engineering, University of Tehran, North Kargar St., 14399-57131 Tehran, Iran² Living Matter Physics, Max Planck Institute for Dynamics and Self-Organization, 37077 Göttingen, Germany³ Living Matter and Biophysics, UNAM-National Nanotechnology Research Center and Institute of Materials Science & Nanotechnology, Bilkent University, Ankara, Turkey

* Author to whom any correspondence should be addressed.

E-mail: bahrami@unam.bilkent.edu.tr**Keywords:** cooperative engulfment, vesicle, nanoparticle, membrane curvature, symmetry breaking, endocytosis, drug deliverySupplementary material for this article is available [online](#)

Abstract

Cellular uptake and expulsion of nanoparticles and viruses often involves a substantial particle concentration at the cell membrane. These particles, many of which are distributed across the cell at relatively large distances, cooperate to enter or exit the cell, highlighting the importance of engulfment cooperativity. Here, we explore the cooperative entry and exit of two and multiple distant nanoparticles to and from curved vesicles, representing cellular endocytosis and exocytosis, respectively. We discover indirect engulfment cooperativity between distant nanoparticles wrapped by vesicles, driven by vesicle curvature, which is absent for particles engulfed by a flat bilayer. For the cooperative entry of two identical particles into the vesicle, we identify a counter-intuitive symmetry-breaking in which one fully-engulfed and one non-engulfed particle is more likely than two fully-engulfed or two non-engulfed particles. As a result, with a high concentration of closely-sized external particles, only half of the particles are expected to be successfully internalized by the vesicle, while the remaining half remains unwrapped, and partially engulfed particles are unlikely. In contrast, the cooperative exit of internal particles from the vesicle is characterized by the simultaneous partial engulfment of the particles that are continuously wrapped by the vesicle. This explains how evolution has harnessed membrane curvature for the simultaneous budding of multiple viral particles, a crucial step in viral infection. Our findings for the cooperative entry of multiple particles have significant implication for achieving efficient drug concentration in drug delivery applications.

1. Introduction

Recent advances in nano biotechnology have led to the design and fabrication of tailored inorganic nanoparticles for a multitude of diagnostic and therapeutic applications such as targeted drug delivery, cancer therapy and cellular imaging [1–7]. To perform their functions, nanoparticles have to enter and exit the cell by crossing the cell membrane. Understanding the underlying physical principles governing the interaction between nanoparticles and membranes is crucial for designing synthetic nanomaterials and dealing with nanotoxicity [1, 8, 9]. Moreover, these principles are equally applicable to the cellular uptake of organic nanoparticles, such as viruses and nutrients as well as to the engulfment of nanoparticles by biomimetic vesicles [10–14].

Nanoparticles predominantly enter or exit the cell through particle engulfment during which the host membrane wraps around the particle, causing deformation of the membrane bilayer. The corresponding increase in the curvature energy of the membrane opposes wrapping and should thus be compensated by the adhesion between the particle and the membrane to facilitate particle engulfment [15–20]. The engulfment of a nanoparticle by the membrane has been shown to depend on the membrane curvature elasticity, on the

strength of membrane-particle adhesion, on the shape [21–28] and size [29–32] of the particle and its rigidity [33–35], and on the overall geometry of the membrane [19, 36]. As shown for gold nanoparticles in HeLa cells [31, 37], these nanoparticles have a typical diameter between 20 and 100 nm interacting with vesicles of diameter 300–500 nm, resulting in a relative particle size of about 0.05–0.3 with respect to the vesicle.

We have recently shown how membrane geometry affects the engulfment of individual nanoparticles [36]. Particles facing flat, non-curved membranes exhibited significantly different engulfment pathways compared to those interacting with positively-curved convex or negatively-curved concave membranes [19, 36]. These cases correspond to particles in contact with flat bilayers and those approaching vesicles, whether from the vesicle's interior or exterior, where the vesicle is curved toward or away from the particle, respectively. We note that these pathways are distinguished by the natural vesicle curvature due to its spherical geometry which is different from the spontaneous curvature that results from membrane asymmetry. Analogous to the cellular uptake of nanoparticle originating from within or outside the cell, the engulfment processes by concave and convex membranes are referred to as exocytosis or endocytosis, respectively, both of which have been extensively investigated both theoretically [29, 30, 38, 39] and experimentally [31, 37, 40]. Accordingly, the engulfment of an individual particle can occur via three distinct pathways: Engulfment by flat bilayers; endocytic engulfment; and exocytic engulfment.

Most biological processes and biomedical applications often involve a considerably large concentration of the nanoparticles exposed to the membrane. Examples include cellular uptake of synthetic nanoparticles [31, 37, 41] as well as viral budding, during which cells must expel numerous virions via exocytic budding to complete the viral replication process [8, 16]. Furthermore, the accumulation and agglomeration of inorganic nanoparticles appear to be essential for providing a sufficiently large dosage of co-exposed particles for effective clinical diagnostic and therapeutic purposes [37, 42]. It is thus crucial to understand the cooperative engulfment of nanoparticles particularly at large particle concentration.

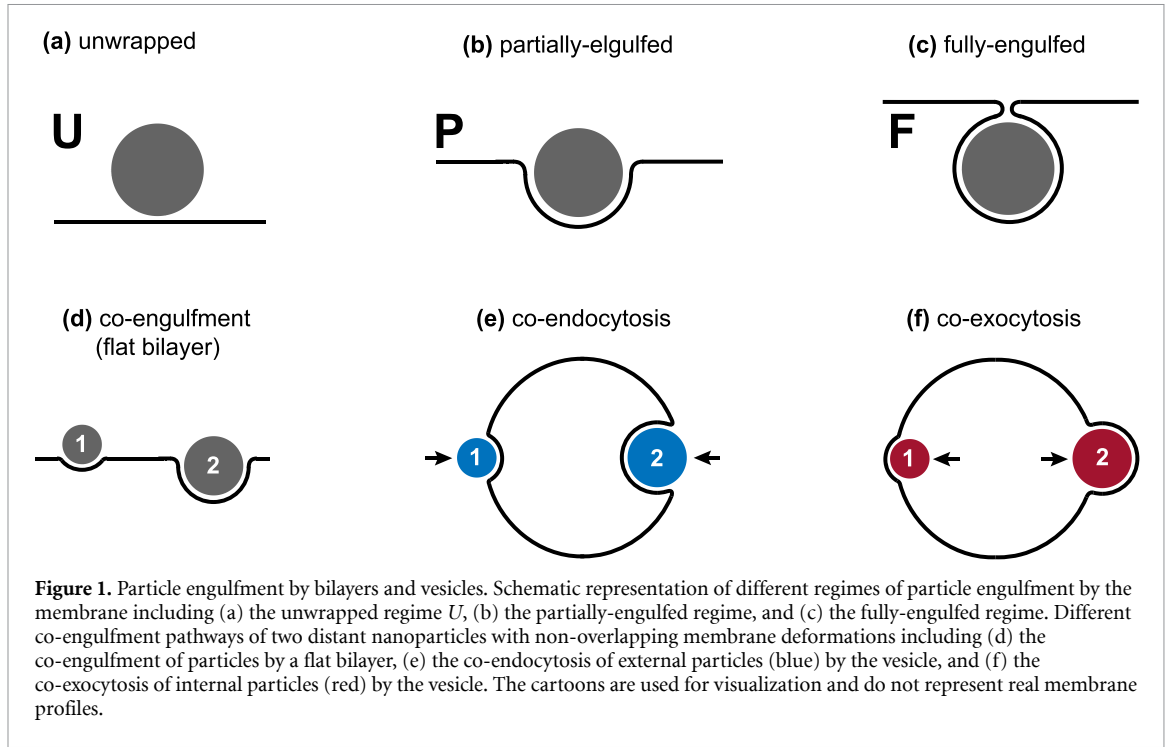
Membrane-mediated cooperativity between nanoparticles at small distances is central to the particle engulfment. Recently, membrane curvature has been found capable of inducing attraction between close nanoparticles and cooperatively wrapping them in tubular invaginations inside the vesicles [43–49]. Computer simulations have provided evidence that curvature-assisted wrapping cooperativity between particles of different sizes facilitates the internalization of small nanoparticles that would otherwise be difficult to wrap [50]. Experimental studies on cooperative cellular uptake of silica nanoparticles with HeLa cells have yielded similar findings [51]. While small particles inhibited the internalization of the larger ones, the larger particles promoted the uptake of the smaller ones. More recently, synergistic nanoparticle wrapping offered an efficient pathway for the uptake of bystander particles [52, 53]. This direct engulfment cooperativity is exclusively experienced by sufficiently close particles whose local membrane deformation overlap, analogous to similar membrane-mediated interactions between adsorbed particles [54–57].

From membrane elasticity perspective, the cellular uptake of multiple distant nanoparticles is assumed to have similar energetic characteristics to that of a single nanoparticle [8]. As a result, thus far membrane-mediated cooperativity between distant particles, referred to as indirect engulfment cooperativity hereafter, has typically been considered insignificant [8].

When a high concentration of nanoparticles is exposed to the membrane, the particles are wrapped by the membrane to varying degrees as observed experimentally [30, 37, 58–61]. These dispersed particles on the membrane surface are often positioned far enough from each other to avoid direct engulfment cooperativity. Therefore, different engulfment proportions of the particles has been related to the critical size for the internalization of the individual particles [19, 36].

In this paper, we use model bilayers and vesicles to systematically study the indirect cooperative engulfment of two and multiple spherical nanoparticles with different sizes. We discover non-trivial indirect wrapping cooperativity in the co-endocytosis of two distant particles, driven by the vesicle curved geometry, which leads to a remarkable symmetry breaking in the engulfment of equally-sized particles. In these circumstances, the particle engulfment by the vesicle is size-independent with no partial engulfment regime observed. Consequently, at higher particle concentrations, only half of the particles are internalized, while the rest remain unwrapped. In contrast, during exocytosis, we observe simultaneous engulfment of the internal particles by the vesicle.

Our paper is organized as follows. We first identify the parameters which determine cooperative engulfment of the particles by bilayers and vesicles. Next, we study the co-engulfment of two particle by flat bilayers followed by the co-endocytosis and co-exocytosis of two particles engulfed by the vesicle. Finally, we extend our results to the general case of the cooperative engulfment of multiple nanoparticles via different engulfment pathways.



2. Results and discussion

Regardless of the engulfment pathway, the engulfment of an individual particle can be categorized into three regimes: The unwrapped regime U ($X = 0$), the partially-engulfed regime P ($0 < X < 1$), and the fully-engulfed regime F ($X = 1$), where the engulfment fraction $X \in [0, 1]$ represents the area fraction of the particle covered by the membrane, see figures 1(a)–(c). Accordingly, for the cooperative engulfment of two distant nanoparticles, we consider three distinct engulfment pathways: Co-engulfment, co-endocytosis and co-exocytosis. The co-engulfment refers to the cooperative engulfment of two distant particles (grey) by flat bilayer membranes (figure 1(d)) while co-endocytosis and co-exocytosis refer to two particles bound to the opposite sides of the vesicle, from the vesicle exterior (blue particles) and interior (red particles) [36], respectively, see figures 1(e) and (f). For each pathway, there are nine possible engulfment regimes, including all dual combinations of the regimes U, P, F for each of the two particles.

The cooperative engulfment of nanoparticles by bilayers and vesicles is governed by the free energy associated with the particles and the membrane. This energy is influenced by various factors, including the geometrical and material properties of the particles and the membrane. These properties are reflected in variables such as particle sizes, vesicle size and volume, membrane bending stiffness, membrane asymmetry, and particle adhesion. Please see the supporting information for more details on free energy components.

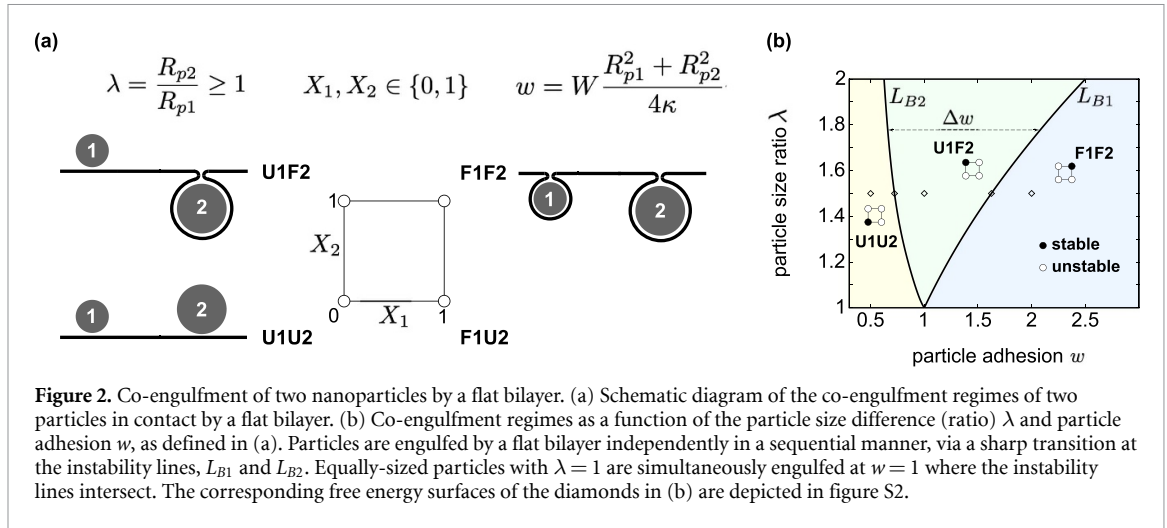
We used homogeneous symmetric membranes with negligible spontaneous curvatures [36, 62]. We also assumed that the vesicle had a low osmotic pressure, enabling free volume adjustment. The theoretical analysis of membrane shapes was performed in a constant area ensemble, where the membrane tension served as a constraint to maintain the membrane area. The vesicle size was thus defined by its constant area $A = 4\pi R_v^2$, determining the vesicle radius R_v . The size of the two spherical nanoparticles with radii R_{p1}, R_{p2} was represented by the average particle size:

$$R_p = \sqrt{\frac{R_{p1}^2 + R_{p2}^2}{2}}. \quad (1)$$

The particle adhesion to the membrane is controlled by the adhesion strength W , which denotes the adhesion energy per unit area of the particle surface.

2.1. The relevant parameters of the cooperative engulfment

Based on geometrical and material variables for the cooperative engulfment of two particles by the vesicle, we introduced dimensionless parameters: The relative size R_p/R_v of the particles with respect to the vesicle; the size difference between the particles represented by their size ratio $\lambda = R_{p2}/R_{p1} \geq 1$ where R_{p1} is the radius of the smaller particle; and the particle adhesion $w = WR_p^2/(2\kappa)$, where the bending rigidity κ of the membrane



defines the energy scale of the system. In the case of a very large vesicle with $R_p/R_v \ll 1$, the vesicle effectively appears flat to the particles. In this limit, R_p/R_v becomes irrelevant, and the cooperative engulfment by the vesicle resembles the co-engulfment by a flat bilayer, parametrized by λ and w .

2.2. Co-engulfment of two nanoparticles by flat bilayers

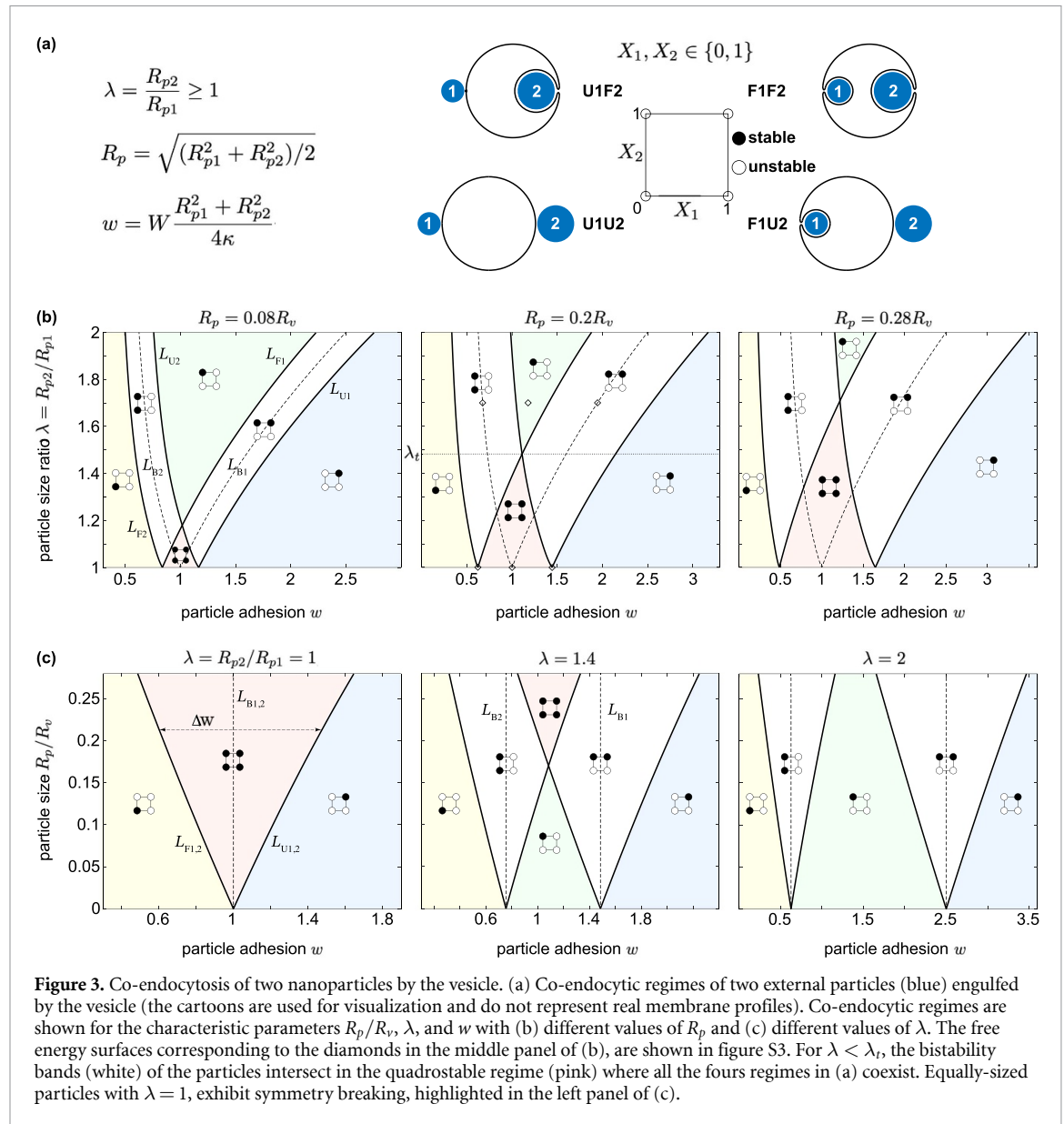
Upon increasing the particle adhesion from small values $w \ll 1$, a single particle on a flat bilayer undergoes a sharp transition from the unwrapped regime U to the fully-engulfed regime F at the transition adhesion $w = 1$, below which the regime F is unstable. Two distant equally-sized particles ($\lambda = 1$), having the same size as the single particle $R_{p1} = R_{p2} = R_p$, exhibit similar simultaneous engulfment at $w = 1$, as seen in figure 2(b). The transition adhesion, $w = 1$, serves as a size-dependent adhesion threshold based on which we define different adhesion regimes for two differently-sized particles with the same average size R_p : The weak adhesion for $w \ll 1$, intermediate adhesion for $w \approx 1$, and strong adhesion for $w \gg 1$. The transition adhesion of the smaller particle, w_1 , is different from that of the larger particle, w_2 :

$$w_1 = \frac{2\kappa}{R_{p1}^2} \frac{R_{p1}^2 + R_{p2}^2}{4\kappa} = \frac{\lambda^2 + 1}{2} \quad (2)$$

$$w_2 = \frac{2\kappa}{R_{p2}^2} \frac{R_{p1}^2 + R_{p2}^2}{4\kappa} = \frac{\lambda^2 + 1}{2\lambda^2}.$$

For different values of λ at a fixed R_p , the loci of w_1 and w_2 define the instability lines, L_{B1} and L_{B2} , of the fully-engulfed regimes of the two particles as displayed in figure 2(b). The two lines intersect at $w = 1$ for equally-sized particles with $\lambda = 1$, while they diverge for larger λ values. The larger particle reaches full engulfment at a lower particle adhesion, $w_2 < w_1$. The instability lines, L_{B1} and L_{B2} , partition the parameter plane w - λ into three engulfment regimes distinguished by different engulfment fractions $X_1, X_2 \in \{0, 1\}$, see figure 2(a). At weak adhesion, both particles remain unwrapped corresponding to the regime $U1U2$ (yellow). At intermediate adhesion, the larger particle is fully engulfed while the smaller one is still unwrapped, denoted by the regime $U1F2$ (green) to the right of L_{B2} . For strong adhesions beyond L_{B1} (blue), both particles are fully engulfed in the regime $F1F2$. Each particle is thus engulfed by the bilayer at its size-dependent individual w_i ($i = 1, 2$) via a sharp transition from the unwrapped to the fully-engulfed regime. Therefore, the engulfment processes of the two particles are independent from each other, showing no engulfment cooperativity. We note that our analysis, here, for the co-engulfment of two nanoparticles by flat bilayers is based on the assumption that the engulfment of the particles is almost independent at relatively far distances without numerical calculation of the corresponding membrane shapes. Indeed, particles on flat bilayers represent particles on a vesicle with very large radius where the vesicle appears as a flat bilayer to the particles.

The co-engulfment of the two particles with a flat bilayer is characterized by specific features. First these particles do not experience partial wrapping which is attributed to the sharp transition between the unwrapped and fully-engulfed regimes. Second, the co-engulfment is size-dependent. As a result, the regime $F1U2$ corresponding to the fully-engulfed smaller particle and the unwrapped larger particle never arises. While equally-sized particles are fully engulfed simultaneously at $w = 1$, the engulfment of differently-sized



particles for larger values of λ occurs sequentially, with increasingly smaller $w_2 < 1$ and larger $w_1 > 1$, and a greater adhesion difference $\Delta w = w_1 - w_2$.

2.3. Co-endocytosis of two nanoparticles by the vesicle

To investigate co-endocytosis, we examined two external particles bound to the opposite sides of the vesicle, see figure 3(a). While a single particle on a flat bilayer is fully engulfed via a sharp transition at $w = 1$, outside the vesicle, the same particle has been demonstrated to exhibit bistability between the unwrapped and fully-engulfed regimes over a range of adhesions [19, 36]. For two particles, we observed a similar behavior resembling a first-order phase transition as seen in the bistability bands (white) in figure 3(b) for three different values of R_p .

The bistability band of particle i ($i = 1, 2$) contains the bistability line L_{Bi} ($i = 1, 2$), where the unwrapped and fully-engulfed regimes of the particle are bistable. These lines (L_{B1} and L_{B2} in figures 3(b) and (c)), coincide with the instability lines observed in the co-engulfment of the same particles by the flat bilayer (equation (2)). Each bistability band is bounded by two lines: L_{Fi} on the left, corresponding to the instability line below which the fully-engulfed regime of particle i becomes unstable, and L_{Ui} on the right, representing the instability line beyond which the unwrapped regime of particle i becomes unstable.

At intermediate adhesion $w \approx 1$, below a transition size ratio, $\lambda = \lambda_t$ (the dotted line in the middle panel of figure 3(b)), the bistability bands of the particles overlap to divide the phase plane into six engulfment regimes with distinct features. For a given R_p at a fixed λ , particles with weak adhesion, corresponding to $w \ll 1$, remain in the unwrapped regime U1U2 (yellow). Upon increasing w , they first enter the bistability

band of the larger particle, where $U1U2$ and $U1F2$ coexist. Depending on λ , further increase in w leads to two distinct regimes separated by the line $\lambda = \lambda_t$. For $\lambda > \lambda_t$, between the non-intersecting bistability bands (green), $U1F2$ becomes stable, where the larger particle is fully engulfed while the smaller one remains unwrapped. For sufficiently closely sized particles with $\lambda < \lambda_t$, in the overlapped region of the bistability bands (pink), a quadrostable regime forms. In this regime, all four metastable states $U1U2$, $U1F2$, $F1U2$, and $F1F2$ coexist (figure 3(a)). Further increase in w takes the particles into the bistability band of the larger particle, where $U1F2$ and $F1F2$ coexist, and eventually into $F1F2$ where both particles are fully engulfed (blue) at strong adhesion $w \gg 1$.

The most intriguing co-endocytic behavior of the particles is observed in the quadrostable regime, at $w \approx 1$ for $\lambda < \lambda_t$. The quadrostable regime is characterized by remarkable features. Similar to the co-engulfment by a flat bilayer, none of the external particles experience partial engulfment by the vesicle. Instead, they exhibit all four possible combinations of U_i and F_j regimes ($i, j = 1, 2$), including the $F1U2$ regime. This regime is not accessible in the co-engulfment by a flat bilayer, nor in co-endocytosis with larger size ratios $\lambda > \lambda_t$, for both of which the two particles are engulfed in a sequential manner following their individual sizes. For these cases, the particle engulfment can serve as a mechanism to distinguish the particles based on their sizes. In the quadrostable regime, however, a surprising situation arises where the vesicle internalizes the particles in a size-independent manner, reflected in the unexpected regime $F1U2$. In addition, the quadrostable regime exhibits the highest level of uncertainty among the four possible regimes, as opposed to the separated bistability bands where each particle coexists in only two regimes. The most interesting feature of the quadrostable regime, however, is the symmetry breaking in the co-endocytosis of equally-sized particles.

2.3.1. Symmetry breaking in the co-endocytosis of identical nanoparticles

The quadrostable regime is bounded, in the parameter phase plane w - λ , by the line $\lambda = 1$ (figure 3(b)) corresponding to equally-sized particles where the engulfment symmetry between the particles is broken. Consequently, the two symmetric engulfment regimes, $U1U2$ and $F1F2$, coexist with the two asymmetric regimes, $U1F2$ and $F1U2$ as displayed in figure S4. The energy barriers separating these regimes vary along the line. At the intersection point of L_{B1} and L_{B2} for $w = 1$, all four regimes have equal energies and are separated by identical energy barriers. Therefore, each of the four regimes is equally likely to occur. At the peak of the energy surface, within the central area of the quadrostable square (figure S4), lies the unstable transition state, $P1P2$, where both particles are partially wrapped to an equal extent. Even for the identical particles, this intuitively-expected regime is unstable.

Symmetry breaking occurs for identical particles along the line $\lambda = 1$, which is a subset of the quadrostable regime (pink) (figure S3(b)). An even more specific situation arises at the point $\lambda = w = 1$, where energy barriers between the four metastable regimes are identical, making them equally likely. This implies that each of the regimes, namely $U1U2$, $U1F2$, $F1U2$, and $F1F2$, is 25% probable. For identical particles, however, the asymmetric regimes, $U1F2$ and $F1U2$, are indistinguishable. Therefore, in the case of two identical external particles on the vesicle, one fully-engulfed and one unwrapped particle (50% probable) is twice as likely as the other two cases of both fully-engulfed (25% probable) or both unwrapped particles (25% probable). In other words, the vesicle tends to fully internalize one particle while retracting the other one, rather than engulfing or retracting both of them simultaneously. Similar behavior is expected along the symmetry breaking line and within the entire quadrostable regime. Overall, for co-endocytosis of two closely sized particles in the intermediate adhesion range, corresponding to the quadrostable regime, one engulfed and one retracted particle is more likely than both being engulfed or both remaining unwrapped.

The quadrostable regime occurs below the transition size difference λ_t which varies by R_p . As seen in figure 3(b), λ_t increases from about 1.2 for $R_p = 0.08R_v$ to about 1.5 for $R_p = 0.2R_v$ and about 1.7 for $R_p = 0.28R_v$. As a consequence, with an increase in R_p , the quadrostable regime expands over a wider range of w , featuring a greater length Δw of the symmetry-breaking line. Similarly the bistability bands shrink for smaller R_p or larger R_v , eventually vanishing for very large vesicles with negligible R_p/R_v , resembling the case of a flat bilayer in figure 2(b). This is manifested in figure 3(c) where the phase diagrams are displayed for different values of λ . The left panel in figure 3(c) corresponds to the particular case of the symmetry breaking for equally-sized particles ($\lambda = 1$) with different R_p values.

2.4. Co-exocytosis of two nanoparticles by the vesicle

The exocytosis of an individual particle has been demonstrated to occur continuously through intermediate partially-engulfed states which form a partial engulfment band [19, 36]. This behavior which resembles a second-order phase transition, is also observed in the co-exocytosis of two internal nanoparticles by the vesicle, as displayed in figures 4(c) and (d). The partially-engulfed regime, P_i , of particle i ($i = 1, 2$) is stable within a particular band in w - λ plane, see figures 4(c) and (d). The left boundary corresponds to the stability

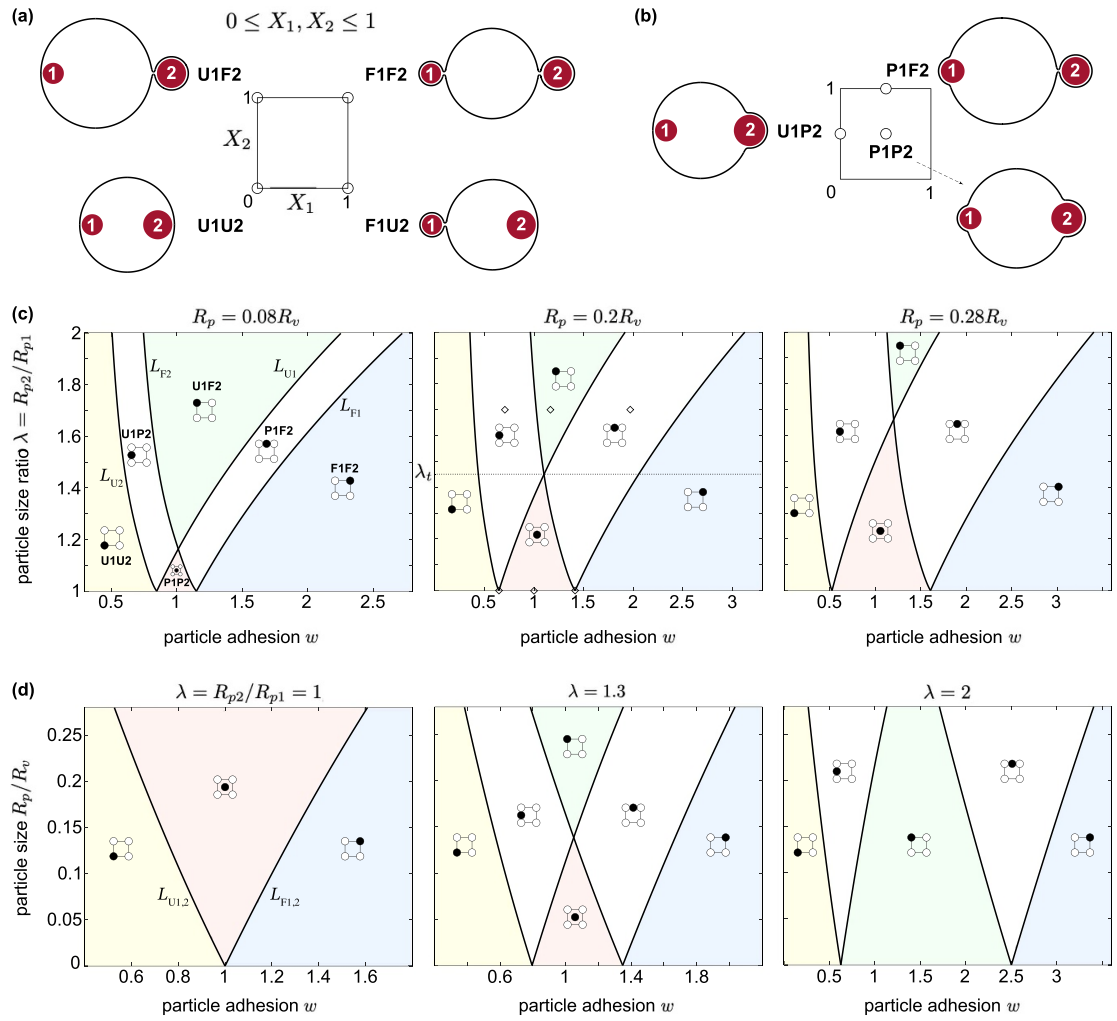


Figure 4. Co-exocytosis of two nanoparticles by the vesicle. (a) Co-exocytic regimes of two internal particles (red) engulfed by the vesicle (the cartoons are used for visualization and do not represent real membrane profiles). Co-exocytic regimes are shown for the characteristic parameters R_p/R_v , λ , and w with (a) different values of R_p and (b) different values of λ . For $\lambda < \lambda_c$, the partial-engulfment bands (white) of the particles intersect in the co-partial-engulfment regime (pink) where the particles are partially engulfed simultaneously. The corresponding free energy surfaces of the diamonds in the middle panel of (c), are shown in figure S5.

line L_{U_i} beyond which the unwrapped regime of particle i becomes stable whereas the right boundary is the stability line L_{F_i} below which the fully-engulfed regime of particle i becomes stable.

The partial engulfment bands partition the w - λ plane into six distinct engulfment regimes. The left and rightmost regimes, $U1U2$ (yellow) and $F1F2$ (blue), and the intermediate regime $U1F2$ (green) between the two bands are similar to those observed in co-endocytosis, see figures 4(c) and (d). The intersection of the two bands for particles with sufficiently small size differences, $\lambda < \lambda_c$, corresponds to the simultaneous partial engulfment of the particles, $P1P2$ (pink), an interesting regime which is neither observed in co-endocytosis nor in the co-engulfment by a flat bilayer. The engulfment fractions of the particles, X_i ($i = 1, 2$), increase with w . In this regime, equally-sized particles undergo symmetric engulfment with $X_1 = X_2 \in (0, 1)$. Similar to the co-engulfment, the size-dependent co-exocytosis does not include the regime $F1U2$. Similar to the quadrostable regime, the simultaneous partial engulfment regime also expands over a wider range of w and λ as R_p increases, as seen in figures 4(c) and (d).

2.5. Stability of co-endocytosed particles

Our quantitative analysis has revealed that the co-endocytic engulfment exhibits metastable regimes, where the unwrapped and fully-engulfed regimes of each external particle coexist within a bistability band in the phase plane w - λ . This bistability band contains the bistability line, where the two regimes have equal energies and the energy barrier is maximal. For a fixed R_p , the height of the maximum energy barriers separating these regimes varies with λ along the bistability lines L_{Bi} ($i = 1, 2$). The stability and lifetime of these metastable regimes depend on the size of the energy barriers.

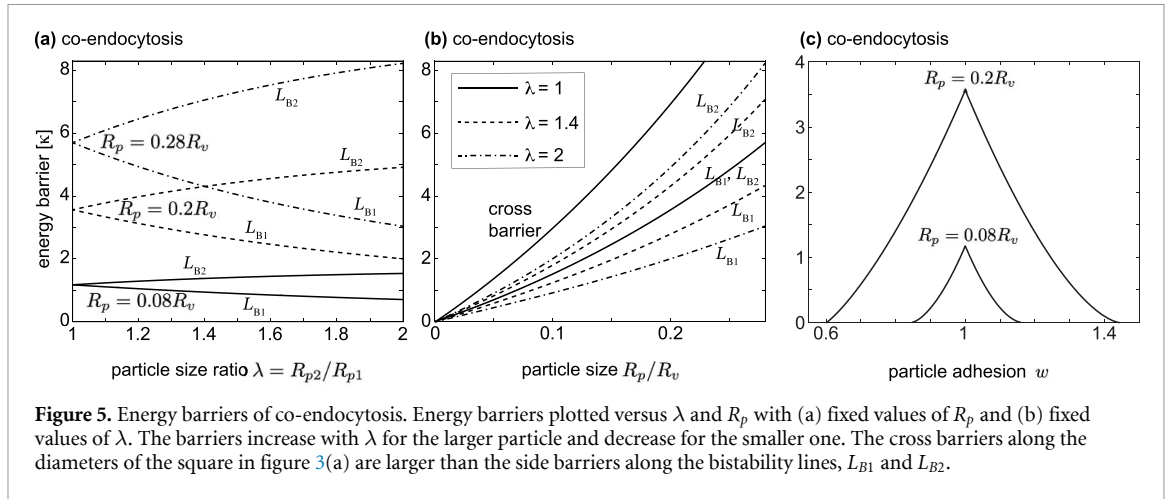


Figure 5(a) displays the two energy barriers along the bistability lines, L_{B1} and L_{B2} , for the co-endocytosis of two particles with three different R_p values, as a function of λ . The energy barrier of the larger particle increases with λ , whereas that of the smaller particle decreases. As a result, for large λ , the energy barrier between the unwrapped and fully-engulfed regimes of the larger particle is significantly greater than that of the smaller particle. For instance, in the case of the largest particles with $R_p = 0.28R_v$, the maximum energy barrier of the larger particle at $\lambda = 2$ is about 8κ , which is significantly higher than the 3κ barrier for the smaller particle, see the dash-dotted curves in figure 5(b).

In figure 5(b), the barriers are plotted against R_p for three different values of λ . Solid lines represent the energy barriers for the special case of equally-sized particles with $\lambda = 1$, corresponding to symmetry breaking. The bottom solid line represents the equal energy barriers along L_{B1} and L_{B2} . The top solid line corresponds to the two equal cross barriers between the two asymmetric regimes, $U1F2$ and $F1U2$, and the two symmetric regimes, $U1U2$ and $F1F2$. The cross barriers are considerably larger than the side barriers along L_{Bi} ($i = 1, 2$). The energy barriers between the four quadrostable regimes, which have equal magnitudes at $\lambda = 1$, exhibit a steady increase with R_p , ranging from small values for negligible R_p to approximately 1.3κ for $R_p = 0.1R_v$ and up to 6κ for the largest particles with $R_p = 0.28R_v$. For a typical membrane bending stiffness of $\kappa = 30 k_B T$, the energy barrier varies from about $40 k_B T$ to $180 k_B T$ for particle sizes in the range $R_p \in [0.1, 0.28]R_v$. The cross barriers are approximately twice as large as the side barriers, exemplified by the cross barrier of about 2.5κ for $R_p = 0.1R_v$.

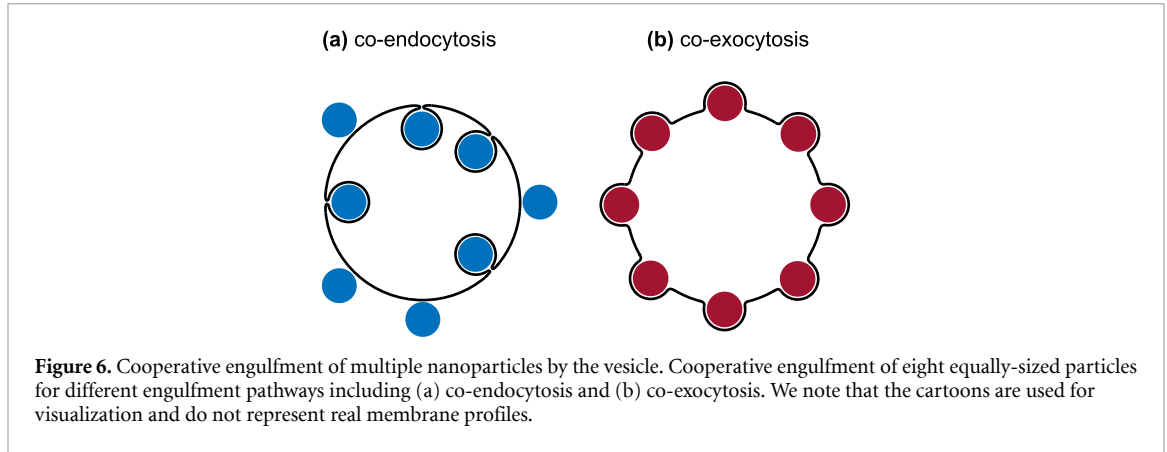
The width of the bistability bands in figure 3(b) reveals how energy barriers vary by w . While the energy barriers are maximal along the bistability lines L_{Bi} ($i = 1, 2$), they vanish on the instability lines L_{Fi} ($i = 1, 2$) and L_{Ui} ($i = 1, 2$) which form the border lines of the bistability bands. Figure 5(c) shows the energy barriers as a function of w for the two relative size $R_p = 0.08R_v$ and $R_p = 0.2R_v$ at $\lambda = 1$ (equally sized particles). The maximal barrier for $w = 1$ reduces almost linearly with both decreasing and increasing w . The range Δw , defined earlier as the maximum width of the quadrostable regime (pink regions in figure 3(b)), determines the adhesion range over which the fully-engulfed and unwrapped states are separated by an energy barrier.

2.6. Cooperative engulfment of multiple particles

To understand the cooperative engulfment of multiple particles, we consider the specific case of n equally-sized particles. In this case, the average particle size R_p is equal to the size R_{pi} of each individual particle:

$$R_p = \sqrt{\frac{1}{n} \sum_{i=1}^n R_{pi}^2} = R_{pi} \quad (i = 1, 2, \dots, n). \quad (3)$$

The complete engulfment of the first particle by the membrane causes the bending energy of the membrane to increase by $8\pi\kappa$. When the particle adhesion is sufficiently large, this energy increase is exactly balanced by a reduction in the adhesion energy (see the supporting information for more details), resulting in the complete engulfment of the particle by the membrane. This complete engulfment is achieved at $w = 1$, regardless of the particle size (provided that the particle is smaller than the vesicle) and whether the particle is engulfed by a flat bilayer or a vesicle, from either the inside or outside. The free energy remains unchanged when additional particles are engulfed at $w = 1$. We note that for a given particle size the number of particles is limited by the size of the vesicle. We also assume that this number is sufficiently small such that the



particles are distant enough to keep overlapping in their local membrane deformations negligible making the results independent from the distances between the particles. Consequently, at $w = 1$, all combinations of n_U unwrapped particles and n_F fully-engulfed particles, with $n_U + n_F = n$, have identical energies. This applies equally to all engulfment pathways including the co-engulfment of multiple particles by a flat bilayer, as well as the co-endocytosis and co-exocytosis of multiple particles by the vesicle. Whereas the unwrapped and fully-engulfed regimes of multiple particles have similar energies in different engulfment pathways, the transition between these regimes and their stability differ significantly across these pathways.

2.6.1. Co-engulfment of multiple particles by the flat bilayer

The co-engulfment of n identical particles by a flat bilayer occurs simultaneously via a sharp transition from the unwrapped regime, $U1U2 \dots Un$, to the fully-engulfed regime, $F1F2 \dots Fn$. The co-engulfment thus involves only two regimes, with a distinct transition between them occurring at $w = 1$, regardless of the number of particles.

2.6.2. Co-endocytosis of multiple particles

The co-endocytosis of n equally-sized particles exhibits a rich polymorphism of $M = 2^n$ engulfment regimes, each consisting of n_F fully-engulfed and $n_U = n - n_F$ unwrapped particles. Figure 6(a) illustrates a sample snapshot of $n = 8$ particles with $n_U = n_F = 4$. At intermediate adhesion with $w = 1$, all these M regimes have equal energies and are thus equally probable. Nevertheless, each combination, $(n_F, n_U = n - n_F)$, has a different frequency and thus a different probability. Out of total M possible regimes, each combination (n_F, n_U) can occur in

$$m(n_F) = \binom{n}{n_F} = \frac{n!}{n_F!(n - n_F)!} = \frac{n!}{n_F!n_U!} \quad (4)$$

different ways where m is a function of n_F , known as the binomial distribution function. The binomial distribution is a symmetric distribution with a peak in the middle at $n_F = n/2$ whose intermediate non-negligible band narrows very rapidly with the increasing number of particles n . Figure S6 illustrates the binomial distribution function for three cases of $n = 10, 100$, and 500 particles as a function of the fraction n_F/n of the fully-engulfed particles. Upon increasing number of particles n , the particular combination $n_F/n = 0.5$, where 50% of the particles are fully-engulfed, becomes increasingly more probable compared to the other combinations. Therefore, for large number of identical external particles exposed to a vesicle, it is extremely probable that half the particles are fully-engulfed by the vesicle while the rest of them remain unwrapped.

For the general case of differently-sized particles, the metastable regimes coexist within an n -dimensional parameter space $(w, \lambda_2 \dots \lambda_n)$, where $\lambda_i = R_{pi}/R_{p1}$ ($i = 1, 2, \dots, n$) and λ_1 is taken to be equal to 1 by definition. In this high-dimensional metastable regime (as a general case of the quadrostable regime), each particle has an equal probability of being unwrapped or fully-engulfed, resulting in maximum uncertainty about the engulfment regime of the particles. Overall, for the closely-distanced particles over a broad range of adhesion $w \approx 1$, the vesicle tends to internalize some particles yet leaves a significant proportion of the particles unwrapped.

2.6.3. Co-exocytosis of multiple particles

Multiple equally-sized particles inside a vesicle, undergo simultaneous partial engulfment at the intermediate adhesions $w \approx 1$. As w increases, the wrapping fractions X_i ($i = 1 \dots n$) steadily increase while the particles

undergo a continuous transition from the unwrapped regime, $U1U2 \dots Un$, through the partial engulfment regime, $P1P2 \dots Pn$, to the full engulfment regime, $F1F2 \dots Fn$. All particles are partially engulfed to the same extent, characterized by identical engulfment fractions $X_i = X_1$ ($i = 2, 3, \dots, n$), as illustrated in figure 6(b) for $n = 8$.

3. Methods

All the information about the methods are found in the supporting information.

4. Conclusion

We study the cooperative entry and exit of nanoparticles and viruses into and from cells by exploring co-endocytic and co-exocytic engulfment pathways.

For co-endocytosis, we discover a quadrostable regime for closely-sized particles at intermediate adhesions, which transitions into a corresponding metastable regime when multiple particles are involved. More interestingly, we show that for equally-sized particles, this results in a non-trivial symmetry breaking. This metastability implies that when there are more than two external particles, the vesicle tends to internalize half of the particles while leaving the rest of them unwrapped. This emerging behavior in the collective engulfment of multiple particles has significant implications.

In many drug delivery applications, where large concentration of nanoparticles are exposed to the cell, the drug dose or the amount of the internalized particles is critical. Our findings have crucial implications for the practical application of nanoparticles in therapeutics and diagnostics, as they can offer valuable design principles for determining the necessary drug carrier or virus dosage required for cell entry.

In experiments with a large concentration of external particles of different sizes in contact with membranes, particles have been observed to be wrapped by the membrane to varying extents, including unwrapped, fully-engulfed, and partially-engulfed particles [31, 37, 60]. This phenomenon has been related to the critical particle size for successful engulfment [19, 36]. We demonstrate that even for equally-sized particles at the critical size, complete internalization is only achieved for about half of the particles. This emerging collective behavior originates from the unusual engulfment cooperativity we unravel here which is not related to the particle size.

We also showed that this collective engulfment with some particles unwrapped and other completely engulfed, is strongly stable. The relatively large energy barriers, ranging from about $40 k_B T$ to $180 k_B T$, calculated here for typical nanoparticles and viruses with sizes in the range of $R_p \in [0.1, 0.28] R_V$, are unlikely to be overcome by thermal fluctuations, resulting in the strong stability of the metastable regimes.

We showed that the co-exocytosis proceeds continuously with simultaneous partial-engulfment of the internal particles and extended our results to the general case of multiple particles. Our findings on simultaneous co-exocytosis of multiple internal nanoparticles through intermediate partially-engulfed regimes explain viral budding. During viral infection a few nano-sized viruses enter the cell via endocytosis. The released virions must then exit the cell to complete the viral replication step, a process which typically occurs simultaneously for several virions [63]. Our results on the co-exocytosis of multiple equally-sized particles reveal the underlying mechanism and energetics of the viral budding by which the cell simultaneously expels these almost identical virions.

Membrane curvature has been found to account for membrane-mediated interactions between adsorbed particles. While cylindrical inclusion adsorbed on flat bilayers are known to repel each other [54, 64], the attractive or repulsive nature of the curvature-induced interactions between spherical particles is not evident [64]. Sufficiently strong curvature has been demonstrated, with theoretical calculations, to induce attraction between the particles [65]. These attractive interactions have not only been approved using coarse-grained molecular dynamics simulations [45] and energy minimization of tessellated vesicles [49] but also observed experimentally [66]. Here, we report long-range curvature-mediated cooperativity between spherical particles on curved vesicles. Our results complement our previous results on short-range curvature-mediated interactions between adsorbed spherical particles on the vesicle [49].

Data availability statement

All data that support the findings of this study are included within the article (and any supplementary files).

Acknowledgments

A H B acknowledges support from the Max Planck Society within the framework of Max Planck Partner Group, and from the European Molecular Biology Organization, Grant EMBO IG 5032.

Conflict of interest

The authors declare no competing interests.

Author contributions

A H B designed research; A B and A H B performed research, analyzed the data, and wrote the article.

ORCID iDs

Arash Bahrami  <https://orcid.org/0000-0002-9222-8795>

Amir H Bahrami  <https://orcid.org/0000-0001-5841-2516>

References

- [1] Nel A E, Mädler L, Velegol D, Xia T, Hoek E M, Somasundaran P, Klaessig F, Castranova V and Thompson M 2009 Understanding biophysicochemical interactions at the nano–bio interface *Nat. Mater.* **8** 543–57
- [2] Peer D, Karp J M, Hong S, Farokhzad O C, Margalit R and Langer R 2007 Nanocarriers as an emerging platform for cancer therapy *Nat. Nanotechnol.* **2** 751–60
- [3] Stoeva S I, Lee J-S, Smith J E, Rosen S T and Mirkin C A 2006 Multiplexed detection of protein cancer markers with biobarcode nanoparticle probes *J. Am. Chem. Soc.* **128** 8378–9
- [4] Rodriguez P L, Harada T, Christian D A, Pantano D A, Tsai R K and Discher D E 2013 Minimal “self” peptides that inhibit phagocytic clearance and enhance delivery of nanoparticles *Science* **339** 971–5
- [5] Rosenblum D, Joshi N, Tao W, Karp J M and Peer D 2018 Progress and challenges towards targeted delivery of cancer therapeutics *Nat. Commun.* **9** 1410
- [6] Mani V, Chikkaveeraiah B V, Patel V, Gutkind J S and Rusling J F 2009 Ultrasensitive immunosensor for cancer biomarker proteins using gold nanoparticle film electrodes and multienzyme-particle amplification *ACS Nano* **3** 585–94
- [7] Bao G, Mitragotri S and Tong S 2013 Multifunctional nanoparticles for drug delivery and molecular imaging *Annu. Rev. Biomed. Eng.* **15** 253–82
- [8] Zhang S, Gao H and Bao G 2015 Physical principles of nanoparticle cellular endocytosis *ACS Nano* **9** 8655–71
- [9] Chen K L and Bothun G D 2014 Nanoparticles meet cell membranes: probing nonspecific interactions using model membranes *Environ. Sci. Technol.* **48** 873–80
- [10] Dimitrov D S 2004 Virus entry: molecular mechanisms and biomedical applications *Nat. Rev. Microbiol.* **2** 109–22
- [11] Yameen B, Choi W I, Vilos C, Swami A, Shi J and Farokhzad O C 2014 Insight into nanoparticle cellular uptake and intracellular targeting *J. Control. Release* **190** 485–99
- [12] Gumz H, Boye S, Iyisan B, Krönert V, Formanek P, Voit B, Lederer A and Appelhans D 2019 Toward functional synthetic cells: in-depth study of nanoparticle and enzyme diffusion through a cross-linked polymersome membrane *Adv. Sci.* **6** 1801299
- [13] Jaskiewicz K, Larsen A, Schaeffel D, Koynov K, Lieberwirth I, Fytas G, Landfester K and Kroeger A 2012 Incorporation of nanoparticles into polymersomes: size and concentration effects *ACS Nano* **6** 7254–62
- [14] Kostina N Y *et al* 2019 Membrane-mimetic dendrimersomes engulf living bacteria via endocytosis *Nano Lett.* **19** 5732–8
- [15] Dasgupta S, Auth T and Gompper G 2017 Nano- and microparticles at fluid and biological interfaces *J. Phys.: Condens. Matter* **29** 373003
- [16] Deserno M 2004 Elastic deformation of a fluid membrane upon colloid binding *Phys. Rev. E* **69** 031903
- [17] Gózdź W 2007 Deformations of lipid vesicles induced by attached spherical particles *Langmuir* **23** 5665–9
- [18] Lipowsky R and Döbereiner H-G 1998 Vesicles in contact with nanoparticles and colloids *Europhys. Lett.* **43** 219
- [19] Agudo-Canalejo J and Lipowsky R 2015 Critical particle sizes for the engulfment of nanoparticles by membranes and vesicles with bilayer asymmetry *ACS Nano* **9** 3704–20
- [20] Frey E, Ziebert F and Schwarz U S 2019 Stochastic dynamics of nanoparticle and virus uptake *Phys. Rev. Lett.* **122** 088102
- [21] Gratton S E, Ropp P A, Pohlhaus P D, Luft J C, Madden V J, Napier M E and DeSimone J M 2008 The effect of particle design on cellular internalization pathways *Proc. Natl Acad. Sci.* **105** 11613–8
- [22] Vácha R, Martínez-Veracoechea F J and Frenkel D 2011 Receptor-mediated endocytosis of nanoparticles of various shapes *Nano Lett.* **11** 5391–5
- [23] Champion J A and Mitragotri S 2006 Role of target geometry in phagocytosis *Proc. Natl Acad. Sci.* **103** 4930–4
- [24] Richards D M and Endres R G 2016 Target shape dependence in a simple model of receptor-mediated endocytosis and phagocytosis *Proc. Natl Acad. Sci.* **113** 6113–8
- [25] Yang K and Ma Y-Q 2010 Computer simulation of the translocation of nanoparticles with different shapes across a lipid bilayer *Nat. Nanotechnol.* **5** 579–83
- [26] Bahrami A H 2013 Orientational changes and impaired internalization of ellipsoidal nanoparticles by vesicle membranes *Soft Matter* **9** 8642–6
- [27] Dasgupta S, Auth T and Gompper G 2014 Shape and orientation matter for the cellular uptake of nonspherical particles *Nano Lett.* **14** 687–93
- [28] Shi X, von Dem Bussche A, Hurt R H, Kane A B and Gao H 2011 Cell entry of one-dimensional nanomaterials occurs by tip recognition and rotation *Nat. Nanotechnol.* **6** 714–9
- [29] Gao H, Shi W and Freund L B 2005 Mechanics of receptor-mediated endocytosis *Proc. Natl Acad. Sci.* **102** 9469–74

- [30] Zhang S, Li J, Lykotrafitis G, Bao G and Suresh S 2009 Size-dependent endocytosis of nanoparticles *Adv. Mater.* **21** 419
- [31] Chithrani B D, Ghazani A A and Chan W C 2006 Determining the size and shape dependence of gold nanoparticle uptake into mammalian cells *Nano Lett.* **6** 662–8
- [32] Shen Z, Ye H, Yi X and Li Y 2018 Membrane wrapping efficiency of elastic nanoparticles during endocytosis: size and shape matter *ACS Nano* **13** 215–28
- [33] Liu X, Auth T, Hazra N, Ebbesen M F, Brewer J, Gompper G, Crassous J J and Sparr E 2023 Wrapping anisotropic microgel particles in lipid membranes: effects of particle shape and membrane rigidity *Proc. Natl Acad. Sci.* **120** e2217534120
- [34] Zou D *et al* 2023 Nanoparticle elasticity regulates the formation of cell membrane-coated nanoparticles and their nano-bio interactions *Proc. Natl Acad. Sci.* **120** e2214757120
- [35] Anselmo A C, Zhang M, Kumar S, Vogus D R, Menegatti S, Helgeson M E and Mitragotri S 2015 Elasticity of nanoparticles influences their blood circulation, phagocytosis, endocytosis and targeting *ACS Nano* **9** 3169–77
- [36] Bahrami A H, Lipowsky R and Weikl T R 2016 The role of membrane curvature for the wrapping of nanoparticles *Soft Matter* **12** 581–7
- [37] Chithrani B D and Chan W C 2007 Elucidating the mechanism of cellular uptake and removal of protein-coated gold nanoparticles of different sizes and shapes *Nano Lett.* **7** 1542–50
- [38] Bao G and Bao X R 2005 Shedding light on the dynamics of endocytosis and viral budding *Proc. Natl Acad. Sci.* **102** 9997–8
- [39] Decuzzi P and Ferrari M 2007 The role of specific and non-specific interactions in receptor-mediated endocytosis of nanoparticles *Biomaterials* **28** 2915–22
- [40] Spanke H T, Style R W, François-Martin C, Feofilova M, Eisentraut M, Kress H, Agudo-Canalejo J and Dufresne E R 2020 Wrapping of microparticles by floppy lipid vesicles *Phys. Rev. Lett.* **125** 198102
- [41] Tay C Y, Setyawati M I and Leong D T 2017 Nanoparticle density: a critical biophysical regulator of endothelial permeability *ACS Nano* **11** 2764–72
- [42] Rees P, Wills J W, Brown M R, Barnes C M and Summers H D 2019 The origin of heterogeneous nanoparticle uptake by cells *Nat. Commun.* **10** 2341
- [43] Koltover I, Raedler J O and Safinya C R 1999 Membrane mediated attraction and ordered aggregation of colloidal particles bound to giant phospholipid vesicles *Phys. Rev. Lett.* **82** 1991–4
- [44] Bahrami A H, Lipowsky R and Weikl T R 2012 Tubulation and aggregation of spherical nanoparticles adsorbed on vesicles *Phys. Rev. Lett.* **109** 188102
- [45] Reynwar B J, Illya G, Harmandaris V A, Müller M M, Kremer K and Deserno M 2007 Aggregation and vesiculation of membrane proteins by curvature-mediated interactions *Nature* **447** 461–4
- [46] Bahrami A H, Raatz M, Agudo-Canalejo J, Michel R, Curtis E M, Hall C K, Gradzielski M, Lipowsky R and Weikl T R 2014 Wrapping of nanoparticles by membranes *Adv. Colloid Interface Sci.* **208** 214–24
- [47] Šarić A and Cacciuto A 2012 Mechanism of membrane tube formation induced by adhesive nanocomponents *Phys. Rev. Lett.* **109** 188101
- [48] Raatz M, Lipowsky R and Weikl T R 2014 Cooperative wrapping of nanoparticles by membrane tubes *Soft Matter* **10** 3570–7
- [49] Bahrami A H and Weikl T R 2018 Curvature-mediated assembly of janus nanoparticles on membrane vesicles *Nano Lett.* **18** 1259–63
- [50] Yue T and Zhang X 2012 Cooperative effect in receptor-mediated endocytosis of multiple nanoparticles *ACS Nano* **6** 3196–205
- [51] Li L, Xi W-S, Su Q, Li Y, Yan G-H, Liu Y, Wang H and Cao A 2019 Unexpected size effect: the interplay between different-sized nanoparticles in their cellular uptake *Small* **15** 1901687
- [52] He K, Wei Y, Zhang Z, Chen H, Yuan B, Pang H-B and Yang K 2021 Membrane-curvature-mediated co-endocytosis of bystander and functional nanoparticles *Nanoscale* **13** 9626–33
- [53] Wei Y, Tang T and Pang H-B 2019 Cellular internalization of bystander nanomaterial induced by TAT-nanoparticles and regulated by extracellular cysteine *Nat. Commun.* **10** 3646
- [54] Weikl T R 2003 Indirect interactions of membrane-adsorbed cylinders *Eur. Phys. J. E* **12** 265–73
- [55] Weikl T R 2018 Membrane-mediated cooperativity of proteins *Annu. Rev. Phys. Chem.* **69** 521–39
- [56] Midya J, Auth T and Gompper G 2023 Membrane-mediated interactions between nonspherical elastic particles *ACS Nano* **17** 1935–45
- [57] Idema T and Kraft D J 2019 Interactions between model inclusions on closed lipid bilayer membranes *Curr. Opin. Colloid Interface Sci.* **40** 58–69
- [58] Le Bihan O, Bonnafous P, Marak L, Bickel T, Trépout S, Mornet S, De Haas E, Talbot H, Taveau J-C and Lambert O 2009 Cryo-electron tomography of nanoparticle transmigration into liposome *J. Struct. Biol.* **168** 419–25
- [59] Michel R, Plostica T, Abezgauz L, Danino D and Gradzielski M 2013 Control of the stability and structure of liposomes by means of nanoparticles *Soft Matter* **9** 4167–77
- [60] Michel R, Kesselman E, Plostica T, Danino D and Gradzielski M 2014 Internalization of silica nanoparticles into fluid liposomes: formation of interesting hybrid colloids *Angew. Chem.* **126** 12649–53
- [61] Montis C, Generini V, Boccalini G, Bergese P, Bani D and Berti D 2018 Model lipid bilayers mimic non-specific interactions of gold nanoparticles with macrophage plasma membranes *J. Colloid Interface Sci.* **516** 284–94
- [62] Helfrich W 1973 Elastic properties of lipid bilayers: theory and possible experiments *Z. Naturforsch. C* **28** 693–703
- [63] Tzlil S, Deserno M, Gelbart W M and Ben-Shaul A 2004 A statistical-thermodynamic model of viral budding *Biophys. J.* **86** 2037–48
- [64] Müller M M, Deserno M and Guven J 2005 Interface-mediated interactions between particles: a geometrical approach *Phys. Rev. E* **72** 061407
- [65] Reynwar B J and Deserno M 2011 Membrane-mediated interactions between circular particles in the strongly curved regime *Soft Matter* **7** 8567–75
- [66] Van Der Wel C, Vahid A, Šarić A, Idema T, Heinrich D and Kraft D J 2016 Lipid membrane-mediated attraction between curvature inducing objects *Sci. Rep.* **6** 32825